Available online at www.sciencedirect.com
ScienceDirect
Journal of Power Sources 178 (2008) 671–676
JOURNAL OF POWER SOURCES
www.elsevier.com/locate/jpowsour

Short communication

Corrosion resistance of chromized 316L stainless steel for PEMFC bipolar plates

K.H. Cho, W.G. Lee, S.B. Lee, H. Jang *

Department of Materials Science and Engineering, Korea University, 1, 5-ga, Anam-dong, Sungbuk-gu, Seoul 136-701, South Korea

Received 20 July 2007; received in revised form 11 September 2007; accepted 14 September 2007
Available online 18 September 2007

Abstract

Corrosion resistance of the chromized 316L stainless steel was studied in a proton exchange membrane fuel cell (PEMFC) operating condition. Cr-rich surface layer was formed by pack cementation technique and electrochemical properties of the chromized surface were examined by potentiodynamic and potentiostatic tests. Results showed that the Cr-rich layers underneath the free surface passivated the surface and protect the surface from corrosion in 0.5 M H_2SO_4 solution at 80 °C. However, the Cr-rich layers showed columnar grains with voids when the stainless steel was pack cemented for an extended period of time, resulting in drastic degradation of corrosion resistance. The optimum condition for the best corrosion resistance in the PEMFC operating condition was obtained without sacrificing the interfacial contact resistance.

Keywords: Bipolar plates; PEM fuel cell; Chromizing; Corrosion; Stainless steel

1. Introduction

The bipolar plates that support the membrane electrode assembly have been considered as one of the main challenging components hindering the fuel cell prosperity. It is well known that they must have multifunctional characteristics such as high corrosion resistance, high mechanical strength, durability against shock, no gas permeability, and easy manufacturing for cost effectiveness [1–4]. Currently, machined graphite composite is widely used as bipolar plates for a PEMFC (proton exchange membrane fuel cell) assembly [1,2]. However, graphite composites have been challenged by metals since the graphite composites have high specific volume, low durability, and high manufacturing cost [1–7]. The metallic bipolar plates, on the other hand, suffer from low corrosion resistance at elevated temperatures that can cause power degradation or cell failure. Various metals such as titanium, aluminum, and stainless steel were tested as possible candidates for bipolar plates [2–8] but a successful application for commercially available PEMFC assemblies has not been reported yet.

Among the candidate metals, stainless steel has been considered as a good candidate because of its suitable physical and mechanical properties with relatively low prices. However, the corrosion resistance of stainless steel has to be improved for successful applications in a commercial PEMFC since the bipolar plate is exposed to acidic environment at elevated temperatures for an extended period of time. Several coating techniques such as chemical vapor deposition (CVD), physical vapor deposition (PVD), plasma coating, electroplating, and surface nitriding have been used to improve corrosion resistance [9–17]. On the other hand, the surface treatment should not decrease the electrical conductivity and the cost for the additional surface modification has to be relatively low. Considering the above-mentioned requirements, the pack cementation technique appears to be an attractive surface treatment to improve corrosion resistance without increasing electrical resistance. The pack cementation technique has been employed extensively to improve corrosion resistance or increasing the surface hardness and the experimental methods and the diffusion mechanism during cementation process is well established [18–23].

In the present work, corrosion resistance of chromized austenitic stainless steel 316L by pack cementation was investigated in a PEMFC operating environment. We focused on the microstructural change of the cemented surface layer

* Corresponding author. Tel.: +82 2 3290 3276; fax: +82 2 928 3584.
E-mail address: hojang@korea.ac.kr (H. Jang).

0378-7753/$ – see front matter © 2007 Elsevier B.V. All rights reserved.
doi:10.1016/j.jpowsour.2007.09.031

Table 1
Chemical composition of SS316L (wt.%)

C	0.02
Si	0.79
Mn	0.9
P	0.032
S	0.009
Ni	10.16
Cr	16.79
Mo	2.00
Fe	Balance

by Cr diffusion and its relation with corrosion resistance, interfacial contact resistance, and stability of current density during PEMFC operation.

2. Experimental

2.1. Materials and pack cementation

A hot rolled 316L austenitic stainless steel sheet with a thickness of 3 mm was used as a substrate for chromizing. The stainless steel was a commercially available product and the composition of the steel is shown in Table 1. The sheet was cut into 20 mm × 20 mm × 3 mm plates for a pack cementation and subsequent corrosion tests. Before the pack cementation, the specimens were polished with #100, #200, #320, #600, #800 SiC abrasive papers and were degreased with acetone using an ultrasonic cleaner and dried in the atmosphere for 24 h to make uniform surface conditions. The powder mix for Cr pack cementation was composed of 50 wt.% of Cr powder (325 mesh), 43 wt.% of Al_2O_3 powder (100 mesh), and 7 wt.% of NH_4Cl powder (Aldrich). The powder mix was homogenized using a ball mill for 12 h. The stainless steel specimen and powder mix were placed in a cylindrical steel container and heat treated in a tube furnace in an Ar atmosphere. The pack was heated from room temperature to 1100 °C at a heating rate of 5 °C min^{-1} and held for 2.5 h, 5 h, and 10 h. After pack cementation, the pack was cooled to room temperature. A procedure showing the chromizing process used in this work is given in Table 2.

Table 2
A pack cementation procedure used in this study

1. Cutting	SS316L stainless steel, 20 mm × 20 mm × 4 mm
2. Polishing	#100∼#800 using SiC abrasive papers
3. Degreasing and cleaning	With acetone using an ultrasonic cleaner for 30 min
4. Mixing	Cr (50 wt.%), Al_2O_3 (43 wt.%), and NH_4Cl (7 wt.%) ball milled for 12 h
5. Pack cementation	1100 °C in Ar gas, heating rate: 5 °C min^{-1}, and heat treatment time: sample 1: 2 h 30 min, sample 2: 5 h, and sample 3: 10 h
6. Degreasing and cleaning	With acetone using an ultrasonic cleaner for 30 min

2.2. Microstructure and composition analysis

The cross section of the stainless steel specimen was examined to investigate structural change of the surface layers during pack cementation using a Horiba EX-200 scanning electron microscope (SEM). Concentration profiles of Fe and Cr across the Cr-rich layer were also analyzed using a JEOL JXA-8900R equipped with electron probe X-ray microanalyzer (EPMA). The surface analysis of the stainless steel specimens after corrosion tests was carried out to validate corrosion effects using a SEM.

2.3. Electrochemical measurements

Potentiodynamic and potentiostatic tests were carried out to evaluate the electrochemical behavior of bare 316L stainless steel and the stainless steel specimens pack cemented for 2.5 h, 5 h, and 10 h at 1100 °C. In order to accelerate the corrosion of the stainless steel in a PEMFCs operating condition, 0.5 M H_2SO_4 solution was used and the electrochemical tests were conducted at 80 °C. A corrosion circuit used in this study consisted of three electrodes: Pt plate as a counter electrode, a saturated calomel electrode as a reference electrode, and a stainless steel specimen as a working electrode. The temperature of the corrosion circuit was maintained using an isothermal bath during electrochemical tests. The pack-cemented stainless steel specimen was covered with epoxy resin for electrical insulating, except for one side for electrochemical measurements. VMP3-CHAZ (Prinston applied research) was used to conduct electrochemical experiments. The potentiodynamic test was carried out to investigate general polarization behavior of stainless steels. The potential was applied from −0.2 V versus open circuit voltage to 1.0 V versus SCE during potentiodynamic tests and the scan rate was set at 1 mV min^{-1}. The potentiostatic polarization was measured for 5 h at +0.6 V_{SCE} by purging O_2 into working electrode to simulate the cathode condition during PEMFC operation and at −0.1 V_{SCE} by purging H_2 to simulate the anode condition.

2.4. Interfacial contact resistance (ICR)

Interfacial contact resistance (ICR) was measured with bare 316L stainless steel and pack-cemented stainless steel specimens. ICR measurements were performed using the Wang's method (Fig. 1) [5]. Electrical current (1 A) was applied via two copper plates by E3610A DC power supply (Hewlett-Packard) and the voltage drop across the specimen was monitored by Agilent 34401A potentiometer. The compaction force ranging from 5 kgf to 50 kgf was applied using K-501H test stand (Attonic) and measured by FB50K push–pull dial gage (Imada).

3. Results and discussion

3.1. Microstructures and concentration profiles

The cross sections of the 316L stainless steels chromized for 2.5 h, 5 h, and 10 h at 1100 °C are shown in Fig. 2. The

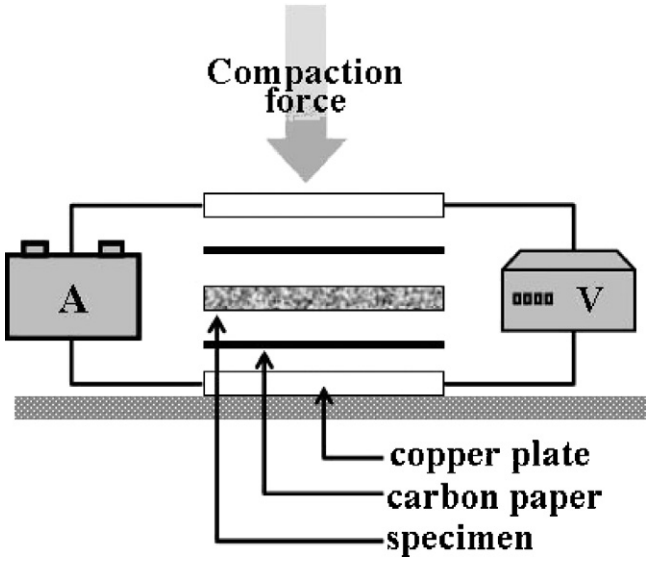

Fig. 1. A diagram showing the measurement for interfacial contact resistance.

figure shows that the microstructure of the chromized surface has been changed since the pack cementation has been carried out at high temperatures. The structural modification includes the grain morphology, atomic structure, and composition. Fig. 2 shows that the specimen exhibits three distinct layers composed of a thin carbide layers, a Cr-rich layer, and substrate layer. The outer thin carbide layer is known as $Cr_{23}C_6$ due to the low carbon content of 316L stainless steel [18].

The specimens that were chromized for 5 h and 10 h exhibited voids, while the same stainless steel chromized for 2.5 h showed no such defects. In the case of specimen chromized for 10 h, columnar grains, which were extended throughout the Cr-rich layer, and large voids were observed. The voids were found both in the Cr-rich layer and the boundary between the Cr-rich layer and the substrate in this case (Figs. 2(c) and 3). On the other hand, the specimen chromized for 5 h showed smaller columnar grains and voids were located near the boundary between the Cr-rich layer and the substrate. Back-scattered electron images at higher magnifications showed the columnar grains (Fig. 3(a)) and voids (Fig. 3(b)) more clearly. The void opened to the free surface was noteworthy because it might affect the corrosion behavior. It was reported that the voids were attributed to the differences of diffusion rates between the elements and is known as a Kirkendall effect [18].

The concentration profiles of Cr as a function of depth were shown in Fig. 4. The thicknesses of the Cr-rich layers were approximately 40 μm, 55 μm, and 50 μm when pack cemented for 2.5 h, 5 h, and 10 h, respectively. The figure indicates that the Cr concentration is the highest near the free surface and gradually decreases until the abrupt drop at the boundary between the Cr-rich layer and the substrate when the specimens were chromized for 2.5 h and 5 h. The estimation from initial Cr concentration of 316L stainless steel and concentration profiles in Fig. 4 suggested that the amount of Cr in the cemented layer after 2.5 h of heat treatment ranged from 53 wt.% at the surface to 33.6 wt.% at the inner boundary. On the other hand, when the specimen was chromized for 10 h no concentration gradient of

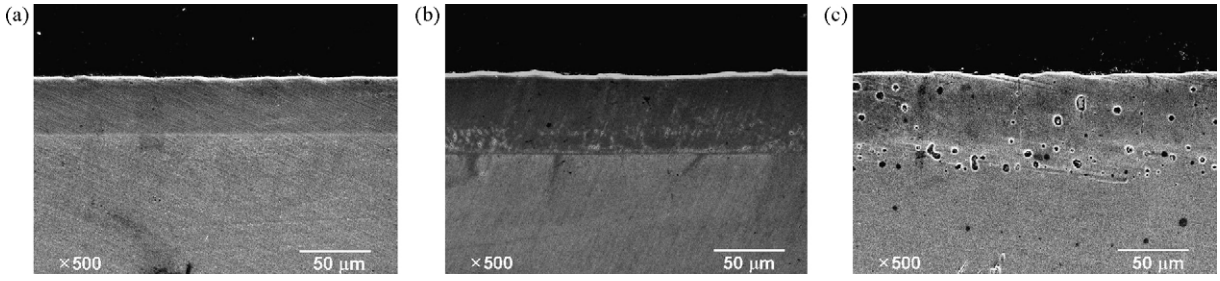

Fig. 2. SEM images showing the cross section of the 316L stainless steel specimen pack cemented for (a) 2.5 h, (b) 5 h, and (c) 10 h.

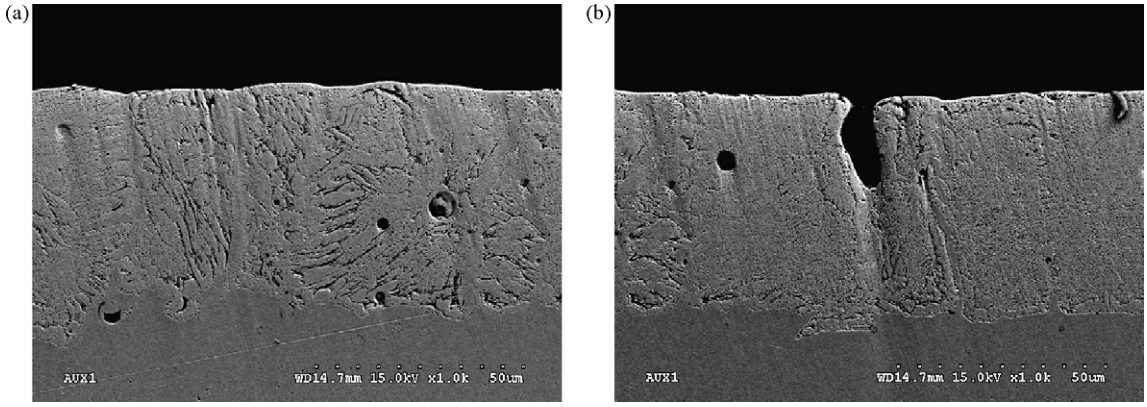

Fig. 3. SEM images (BEI mode) of the Cr-rich layer after chromizing for 10 h at 1100 °C showing columnar grain boundary (a) and a void opened to a free surface (b).

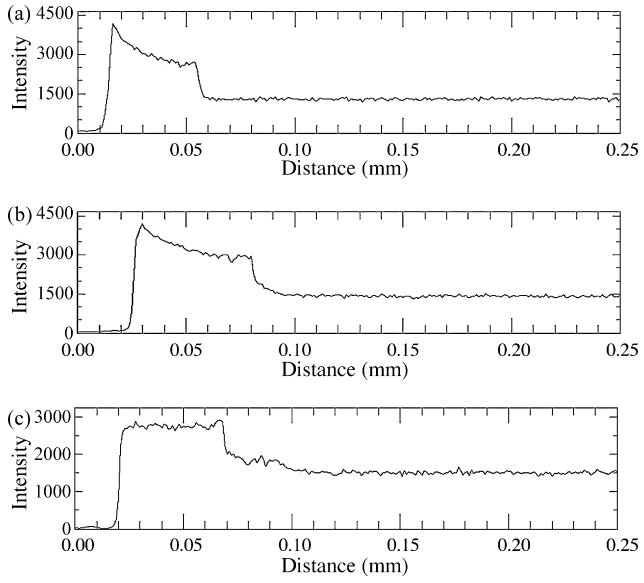

Fig. 4. Concentration profiles of Cr across the Cr-rich layer of stainless steel after pack cemented for (a) 2.5 h, (b) 5 h, and (c) 10 h at 1100 °C.

Cr was observed. This indicates that the Cr diffusion from surface was retarded by the lack of Cr source in the powder pack after a certain period of time and further reaction in the Cr-rich layer was proceeded by Cr self-diffusion without external Cr supply. In this case, the Cr concentration of the Cr-rich layer was lower than the other two cases and many voids were found in the Cr-rich layer and near the boundary between the Cr-rich layer and the substrate. The elemental mapping of Cr and Fe in the Cr-rich layer also showed that the Cr concentration was high

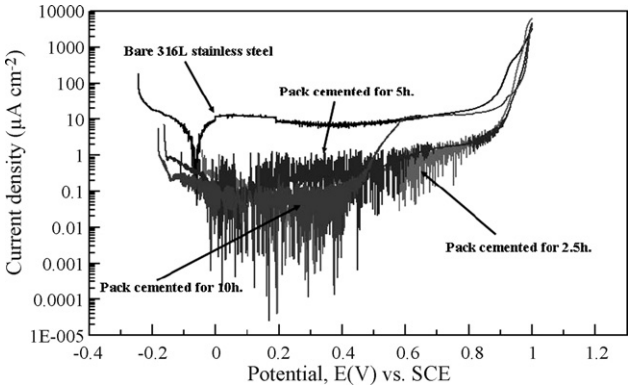

Fig. 6. Potentiodynamic curves from the bare and the pack-cemented 316L stainless steels measured in 0.5 M H_2SO_4 at 80 °C.

near the surface when the Cr cementation was carried out for less than 5 h (Fig. 5). Fig. 5 also shows that the abrupt concentration drop at the phase boundary between α-Fe (Cr-rich layer) and γ-Fe (substrate) disappeared and changed into a diffuse boundary when the cementation was carried out for 10 h [19,21].

3.2. Potentiodynamic tests

A potentiodynamic test was carried out to investigate polarization behavior of bare 316L stainless steel and pack-cemented stainless steel. Fig. 6 shows the polarization curves of the specimen measured in 0.5 M H_2SO_4 solution at 80 °C. The polarization curves of all the specimens clearly exhibit the passive and transpassive regions, while pack-cemented steels exhibit large current density oscillation. The polarization curves of the 316L

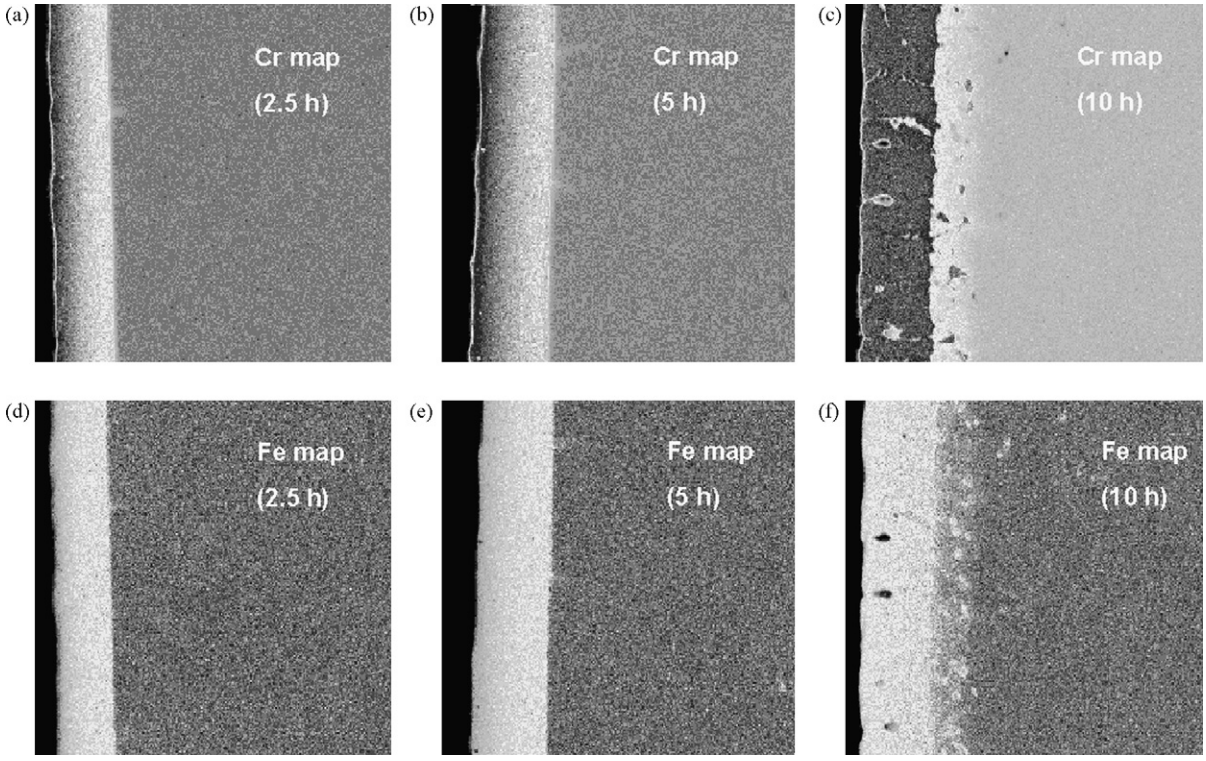

Fig. 5. Cr map (a–c) and Fe map (d–f) of the stainless steel specimen after pack cemented for (a) 2.5 h, (b) 5 h, and (c) 10 h.

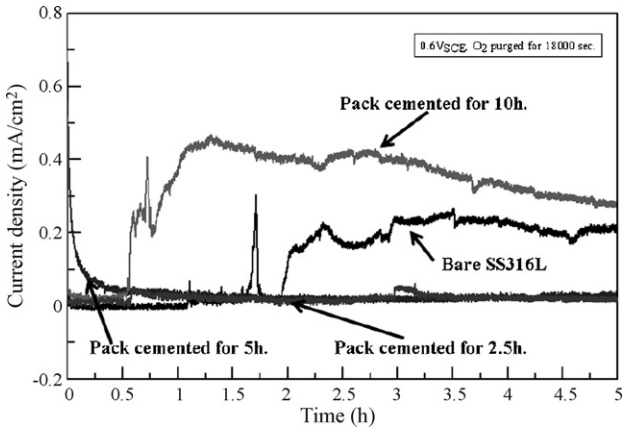

Fig. 7. Potentiostatic curves from the bare and the pack-cemented 316L stainless steels measured at 0.6 V_{SCE} with O_2 purging.

stainless steel chromized for 2.5 h and 5 h show lower current densities than bare 316L stainless steel, suggesting that the Cr cementation can improve the corrosion resistance. On the other hand, when the 316L stainless steel was chromized for 10 h, it exhibits two passive and transpassive regions with unstable electrochemical behavior at high potential. The current density in the first passive region is similar with those of other pack-cemented stainless steels but the current density in the second passive region is similar to that of bare 316L stainless steel indicating that the chromized layer is no longer effective to protect the stainless steel from corrosion. The figure clearly indicates that the current density of pack-cemented stainless steels at 0.6 V_{SCE}, which is a cathodic operating potential in a PEMFC, are lower than that of bare 316L stainless steel except in the case of pack-cemented specimen for 10 h.

3.3. Potentiostatic tests

In order to examine the current density during PEMFC operation, potentiostatic tests were conducted using 0.5 M H_2SO_4 solution at 80 °C for 5 h. The potential of 0.6 V_{SCE} was loaded and O_2 gas was purged to the working electrode to simulate the cathode environment of PEMFC. The potential of −0.1 V_{SCE} was applied to simulate anode environment by purging H_2 gas to the working electrode. The current density of specimens as a function of time was measured in the cathode environment (0.6 V_{SCE} and O_2 purging) and plotted in Fig. 7. The current density of pack-cemented stainless steel for 2.5 h and 5 h exhibits low stable values during the whole experiments. However, bare 316L stainless and pack-cemented specimens for 10 h showed an abrupt increase of current density in the middle of potentiostatic experiments. In particular, it was interesting to observe the sudden increase of the current density found in the case of the specimen chromized for 10 h, while other specimens maintained low current density for up to 2 h.

The higher current density of these specimens during potentiostatic tests can be associated with the polarization behavior obtained from potentiodynamic tests in Fig. 6 since the current density of bare 316L stainless steel and pack cemented for 10 h stainless steel at 0.6 V_{SCE} exhibits higher values than other pack-cemented stainless steel. The surface morphology of the stainless steel was examined before and after the corrosion test using an SEM. Fig. 8 shows the surfaces of the bare specimen and the pack-cemented specimens after corrosion tests for 10 h at 0.6 V_{SCE} with O_2 purging gas. They show pits and voids opened to the surface, which cause an abrupt increase of current density during potentiostatic tests. On the other hand, the surface defects were not observed in the specimens pack cemented for 2.5 h and 5 h, suggesting that the surface defects affect the stability of current density during potentiostatic tests. The microstructural features of the 316L stainless steel chromized for 10 h (Figs. 3 and 5) also support the early degradation of corrosion resistance. This is because the grain boundaries of the columnar grains provide fast diffusion paths during corrosion and the voids present in the Cr-rich layer accelerate the corrosion rate by pitting corrosion mechanism. On the other hand, all the specimens tested in the simulated anode condition did not show any surface corrosion. This is because the H_2 gas purged in a solution provides a reduction environment around the working electrode while O_2 gas activates corrosion reaction [24].

3.4. Interfacial contact resistance

The interfacial contact resistance (ICR) between specimens and carbon paper as a function of the compaction force is shown

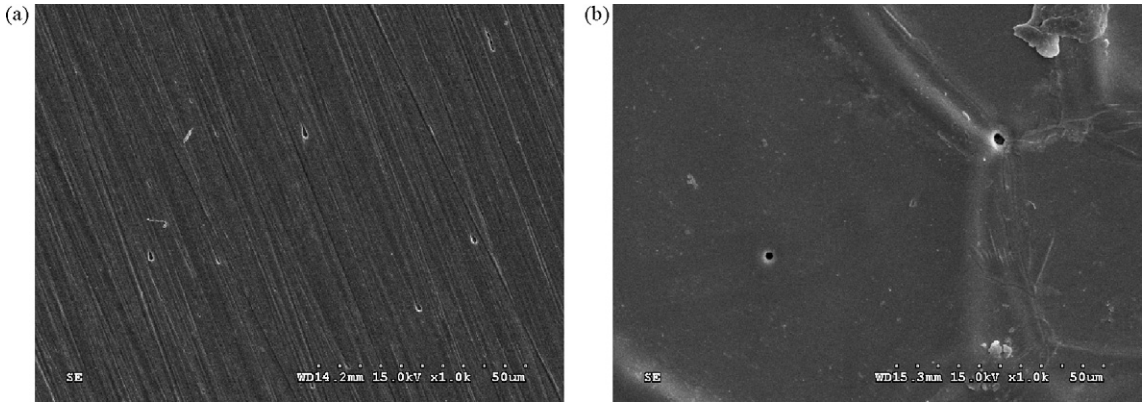

Fig. 8. Surface images of the bare 316L stainless steel (a) and the stainless steel pack cemented for 10 h (b) after potentiostatic tests at 0.6 V_{SCE} with O_2 purging.

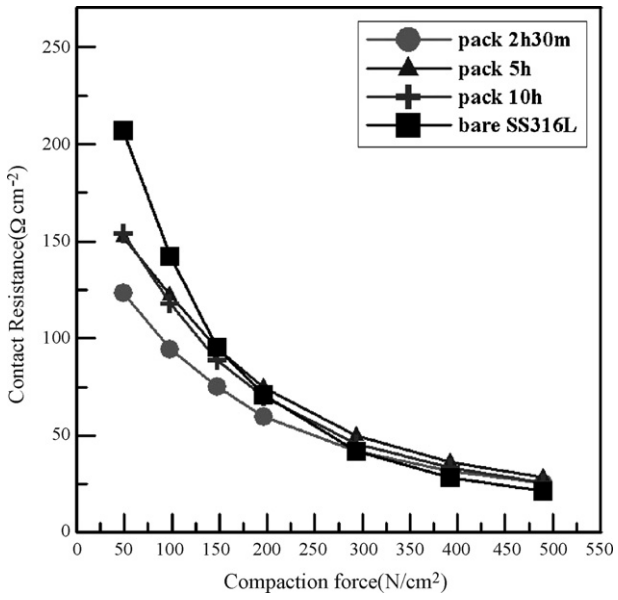

Fig. 9. Interfacial contact resistances as a function of compaction force.

in Fig. 9. The ICR of all the specimens decreases with increasing compaction force due to the increase of the real contact area. The measured data indicates that all the pack-cemented stainless steel specimens exhibit lower ICR values than bare 316L stainless steel in low compaction force (50–300 N cm^{-2}). However, the ICR values of all specimens become similar when the compaction force reaches 300 N cm^{-2} and beyond. This is because of the grain growth occurred during pack cementation and by offsetting the possible increase of the ICR by cemented Cr-rich layers. Among the pack-cemented stainless steels, the specimen of 2.5 h pack cementation shows the lowest ICR value than other specimens. This result also coincides with the microstructure of the cemented stainless steel since the Cr-rich layer with voids increases the electrical resistance.

4. Conclusions

316L austenitic stainless steel was chromized by pack cementation at 1100 °C for 2.5 h, 5 h, and 10 h. The composition profiles showed the formation of Cr-rich layers in the pack-cemented stainless steels. The stainless steel chromized at 1100 °C for 10 h form voids and exhibited a diffuse boundary between the Cr-rich layer and the substrate. The polarization curves measured at 80 °C in 0.5 M H_2SO_4 solution showed that the corrosion resistance was improved after pack cementation. However, when the cementation was carried out for an extended period of time (for 10 h), the current density at 0.6 V_{SCE} became similar to bare 316L stainless steel, indicating that no effective protection against corrosion. The chromized stainless steel with 2.5 h cementation, on the other hand, exhibited low current density and stable polarization behavior. The interfacial contact resistance was decreased with increase of compaction force and pack-cemented stainless steels exhibited similar level of ICR compared to bare stainless steel when compaction force was applied more than 300 N cm^{-2}.

Acknowledgement

This work was supported by the grants from the Seoul R&BD Program at Korea University.

References

[1] W. Vielstich, H.A. Gasteiger, A. Lamm, Handbook of Fuel Cells—Fundamentals, Technology and Applications, vol. 3, John Wiley & Sons, 2003 (Chapter 23).
[2] H. Tawfik, Y. Hung, D. Mahajan, J. Power Sources 163 (2007) 755–767.
[3] B.D. Cunningham, J. Huang, D.G. Baird, Int. Mater. Rev. 52 (2007) 1–13.
[4] V. Metha, J.S. Cooper, J. Power Sources 114 (2003) 32–53.
[5] H. Wang, M.A. Sweikar, J.A. Turner, J. Power Sources 115 (2003) 243–251.
[6] D.P. Davies, P.L. Adcock, M. Turpin, S.J. Rowen, J. Appl. Electrochem. 30 (2000) 101–105.
[7] H. Wang, J.A. Turner, J. Power Sources 128 (2004) 193–200.
[8] D.R. Hodgson, B. May, P.L. Adcock, D.P. Davies, J. Power Sources 96 (2001) 233–235.
[9] M.P. Brady, K. Weisbrod, I. Paulauskas, R.A. Buchanan, L.L. More, H. Wang, M. Wilson, F. Garzon, L.R. Walker, Scripta Mater. 50 (2004) 1017.
[10] M.P. Brady, K. Weisbrod, C. Zawodzinski, I. Paulauskas, R.A. Buchanan, L.R. Walker, Electrochem. Solid State Lett. 5 (2002) A245.
[11] R.J. Tian, J.C. Sun, L. Wang, J. Power Sources 163 (2007) 719–724.
[12] D.G. Nam, H.C. Lee, J. Power Sources 170 (2007) 268–274.
[13] Y. Wang, D.O. Northwood, J. Power Sources 165 (2007) 293–298.
[14] M. Li, S. Luo, C. Zeng, J. Shen, H. Lin, C. Cao, Corros. Sci. 46 (2004) 1369–1380.
[15] E.A. Cho, U.S. Jeon, S.A. Hong, I.H. Oh, S.G. Kang, J. Power Sources 142 (2005) 177–183.
[16] M.P. Brady, K. Weisbrod, I. Paulauskas, R.A. Buchanan, K.L. More, H. Wang, M. Wilson, F. Garzon, L.R. Walker, Scripta Mater. 50 (2004) 1017–1022.
[17] M.A. Lucio Garcia, M.A. Smit, J. Power Sources 158 (2006) 397–402.
[18] Y.D. Kogan, B.P. Sereda, E.P. Kostogorov, Met. Sci. Heat Treat. 36 (1994) 135–139.
[19] M. Zheng, R.A. Rapp, Oxid. Met. 49 (1998) 19–31.
[20] C.A.C. Sequira, C.M.G.S. Nunes, Surf. Eng. 3 (1987) 247.
[21] D.M. Miller, S.C. Kung, S.D. Scarberry, R.A. Rapp, Oxid. Met. 29 (1988) 239–254.
[22] R. Bianco, M.A. Harper, R.A. Rapp, JOM 43 (1991) 20–25.
[23] B.N. Azamasov, R.A. Mel'nikov, Met. Sci. Heat Treat. 36 (1994) 5–6.
[24] Y. Wang, D.O. Northwood, Electrochim. Acta. 52 (2007) 6793–6798.